Research article

Synthesis of glutamine-based green emitting carbon quantum dots as a fluorescent nanoprobe for the determination of iron (Fe^{3+}) in *Solanum tuberrosum* (potato)

Olanrewaju A. Aladesuyi [a,b], Oluwatobi S. Oluwafemi [a,b,*]

[a] *Department of Chemical Sciences, University of Johannesburg, P.O. Box 17011, Doornfontein 2028, Johannesburg, South Africa*
[b] *Centre for Nanomaterials Science Research, University of Johannesburg, P.O. Box 17011, Doornfontein 2028, Johannesburg, South Africa*

A B S T R A C T

Herein, we reported the use of *N*-doped green-emitting carbon quantum dots (*N*-CQDs) as a fluorescent probe for determining of Fe^{3+} ions in *Solanum tuberosum* for the first time. The *N*-CQDs were synthesised through an efficient, one-step, and safe hydrothermal technique using citric acid as the carbon source and glutamine as a novel nitrogen source. The temporal evolution of the optical properties was investigated by varying the synthetic conditions with respect to temperature (160 °C, 180 °C, 200 °C, 220 °C and 240 °C) and citric acid: glutamine precursor ratio (1:1, 1:1.5, l.2,1:3 and 1:4). The *N*-CQDs was characterised using Fourier-Transform Infrared Spectroscopy (FTIR) High-resolution transmission electron microscope (HRTEM), ultraviolet–visible spectroscopy (UV–vis) and X-Ray diffraction analysis (XRD) while its stability was evaluated in different media; NaCl, Roswell Park Memorial Institute (RPMI) and Phosphate Buffered Saline (PBS), and at different pHs. The *N*-CQDs displayed green (525 nm) emission and were spherical with an average particle diameter of 3.41 ± 0.76 nm. The FTIR indicated carboxylic, amino, and hydroxyl functional groups. The as-synthesised *N*-CQDs were stable in NaCl (up to 1 M), RPMI, and PBS without any significant change in its fluorescent intensity. The pH evaluation showed pHs 6 and 7 as the optimum pHs, while the fluorometric analysis showed selectivity towards Fe^{3+} in the presence and absence of interfering ions. The detection limit of 1.05 µM was calculated, and the photoluminescence mechanism revealed static quenching. The *as*-synthesised *N*-CQDs was used as a fluorescent nanoprobe to determine the amount of Fe^{3+} in *Solanum tuberosum* (Potatoes) tubers. The result showed a high level of accuracy (92.13–96.20%) when compared with an established standard analytical procedure with excellent recoveries of 99.23–103.9%. We believe the *as*-synthesised *N*-CQDs can be utilised as a reliable and fast fluorescence nanoprobe for the determining of Fe^{3+} ions.

1. Introduction

Iron, Fe^{3+} is very vital to nature. Physiological processes such as oxygen uptake, oxygen metabolism, electron transfer, and metabolism all require this all-important transition metal [1]. Iron deficiency in the living systems can lead to certain disorders such as

---

anaemia, liver disease, heart failure, and other biological disorders [2]. At the same time, excess iron in the body system is counterproductive. Life-threatening diseases such as cancer, Alzheimer and Parkinson diseases can occur because of iron overload [3]. The report has shown that 30% of the world's population suffers from iron imbalance [4]. Therefore, the need for adequate detection and monitoring of iron levels is highly demanded for human health and safety. In addition, Fe^{3+} is a major source of water and land pollution inimical to human health and safety [5]. Conventional analytical techniques have been used for the determination of Fe^{3+} ions. They include; atomic absorption spectroscopy [6], inductive coupled plasma mass spectroscopy [7], electrochemical analysis etc. Although these techniques are reliable, stable, and sensitive, they require expensive instruments, tedious procedures, complex sample preparation, and are time-consuming. Recently the use of fluorescent sensors for the detection of metal ions (Fe^{3+}, Hg^+, Cu^{2+}) has gained much attention due to the ease of operation, reproducibility, and low cost of operation [8,9].

The choice of an appropriate fluorescent material is critical when fabricating fluorescent sensing systems. Fluorophores, such as organic dyes [10], biological fluorophores [11], oxides nanoparticles [12], and quantum dots [13], have been employed as sensors due to their special fluorescent properties. Nonetheless, they possess shortcomings, such as poor solubility, photobleaching, instability, and toxicity, which hinder their extensive applications. Carbon quantum dots (CQDs) are a class of fluorescent nanomaterials that have attracted much attention owing to their excellent properties, which makes them an ideal candidate for different applications [14–21]. Carbon quantum dots have recently been among the most widely used materials as fluorescent sensors for the detection of metal ions with high sensitivity [22–24]. To improve the fluorescent performance of CQDs in detecting trace metal ions, metal and non-metallic heteroatoms have been doped into the CQDs. However, drawbacks such as toxicity and non-uniformity in doping have limited the use of metals as a dopant. Thus, non-metals such as nitrogen have been widely employed to prepare doped CQDs for metal ion sensing applications [25–28]. Deng et al. [29] synthesised nitrogen-doped CQDs by hydrothermal method using biomass tar and ethylenediamine as precursors. The obtained *N*-CQDs are spherical and showed good feasibility as a fluorescent probe for determining Fe^{3+}. In another study, Zhao et al. carried out the synthesis of *N*-doped blue-emitting CQDs using chitosan as both nitrogen and carbon sources [30]. However, preparing *N*-CQDs emitting in the visible region will be highly desirable for extensive applications. In addition, the use of carbon quantum dots-based fluorescent nanosensors for detecting iron in actual food samples has rarely been reported.

Solanum tuberosum (potatoes) is the third most-consumed food in the world, with an annual consumption of about 374 metric tonnes [31]. Significant variations in the iron content of potatoes because of genotype, soil acidity or alkalinity and environmental factors have raised concerns about the safety and quality of this ever-important staple food. Thus, effective monitoring of iron content in potatoes can go a long way in reducing malnutrition and improving the quality of life in places with high potato consumption. In addition, control of diseases caused by iron deficiency, such as anaemia and stunted growth, will be effectively controlled if the amount of iron in potatoes can be monitored through simple methods like fluorescence sensing.

In this study, we reported the hydrothermal synthesis of green-emitting *N*-CQDs using citric acid as the carbon source and glutamine as the nitrogen source. Glutamine, a non-essential amino acid, is accessible and available naturally in standard diets such as beef, eggs, yogurt, seafood, etc. In addition, glutamine has been adjudged to be non-toxic at controlled concentrations [32]. The ease of accessibility and non-toxicity of glutamine inform its choice as a nitrogen source for CQDs synthesis. The hydrothermal method has the following advantages when compared to other synthetic approaches. This includes, low cost, ease of operation, ecofriendliness, and minimal or no toxicity [33,34]. In addition, the CQDs obtained are photostable and monodispersible [35]. The temporal evolution of the optical properties was investigated by varying the synthetic conditions with respect to temperature and citric acid: glutamine precursor ratio. In addition, the performance of the *as*-synthesised *N*-CQDs in the fluorescent sensing of Fe^{3+} in the presence and absence of other interfering ions was investigated. The *N*-CQDs were found to selectively detect Fe^{3+} in the presence of other metal ions with a low detection limit of 1.05 μM. In addition, media stability of the as-synthesised *N*-CQDs was determined in RPMI, PBS, and NaCl media. The *N*-CQDs were stable in these media as there was little or no change in the fluorescent intensity after several hours. Also, the photostability of the as-synthesised *N*-CQDs was studied through their continuous exposure to UV light. There was no significant change in the fluorescent intensity even after 6 h of continuous irradiation. Furthermore, the as-synthesised *N*-CQDs was used as a fluorescent probe to determine the amount of Fe^{3+} in *Solanum tuberosum* (Potatoes) tubers. To the best of our knowledge, this is the first time an attempt has been made to determine a potato's iron content using a flouronanosensor. The similarity in the result obtained to that of inductively coupled mass spectroscopy (ICPMS), an established procedure, further affirms the feasibility and accuracy of the process.

2. Experimental

2.1. Materials and reagent

Citric acid, glutamine, sodium hydroxide, sulphuric acid, n-butanol, $Cr(NO_3)_3$, $Fe(NO_3)_3$, $Co(NO_3)_2$, $Cd(NO_3)_2$, $Zn(NO_3)_2$, $Pb(NO_3)_2$, NaCl and KCl were purchased from Sigma Aldrich. Potato tubers were purchased from Shoprite supermarket in Johannesburg. All materials were used as purchased without any further purification. Deionized water was used as the solvent throughout the experiment.

2.2. Synthesis of carbon quantum dot

The synthesis of *N*-CQDs was carried out using a one-step hydrothermal facile method. Briefly, 1.152 g (6 mmol) of citric acid and 2.628 g (18 mmol) of glutamine were dissolved in 20 mL of deionized water under slight stirring until a homogenous mixture was formed. The mixture was transferred and sealed in a Teflon-lined stainless-steel autoclave and heated in an oven at 160, 180, 200, 220

and 240 °C for 4 h, separately. The reaction solution was allowed to cool naturally. The yellowish solution was centrifuged for 15 min at 10,000 rpm to separate the undissolved precursors and large particles. After this, the supernatant was washed with n-butanol several times to removed dissolved impurities. The resultant solution was filtered in a 0.02 μm filter paper and freeze-dried to give solid *N*-CQDs crystals. The experiment was repeated at 200 °C to investigate the effect of the citric acid: glutamine ratio on the luminescence intensity.

2.3. Characterisation of N-CQDs

The morphology and particle size of the *N*-CQDs were obtained with a JOEL (JEM 2100) high-resolution transmission electron microscope (HRTEM) at an accelerating voltage of 200 kV. A Spectrum Two PerkinElmer Fourier transforms infrared instrument fitted with an attenuated total reflection sample holder with a scanning range of 400–4000 cm^{-1} was used to investigate the surface chemistry. The fluorescence spectrum and fluorescent lifetime were obtained with an FS5 spectrofluorometer (Edinburg instruments) at 450 nm excitation wavelength. The Ultraviolet–visible (UV–vis) absorption spectra were monitored in 1-cm quartz cuvettes at room temperature (20 °C) using the double beam *S*P-UV 500 spectrophotometer (PerkinElmer). X-ray diffraction (XRD) analysis of the *N*-CQDs was carried out using Brucker D8 Advance diffractometer with monochromatic CuK$_{\alpha 1}$ radiation (λ = 1.5418 Å).
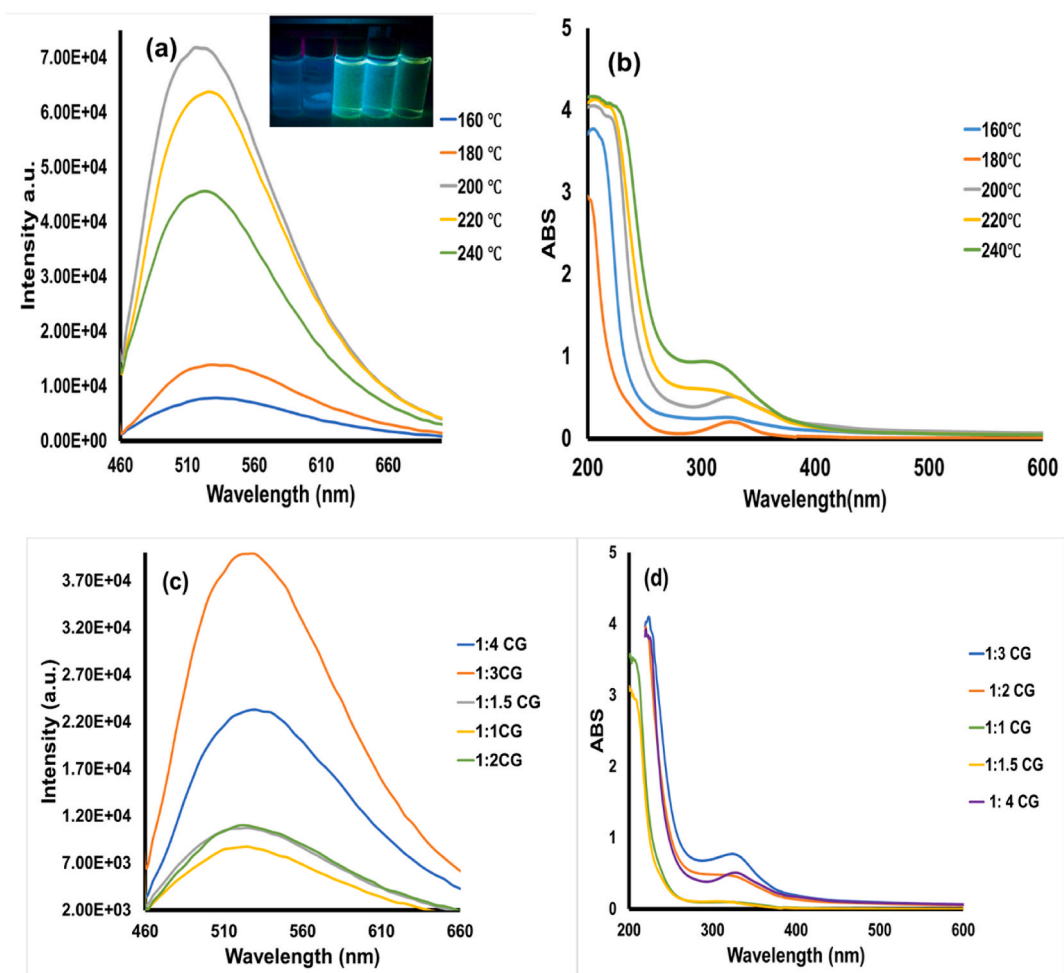


*CG- citric acid: glutamine

Fig. 1. (a) PL spectra of the *as*-synthesised *N*-CQDs at the different reaction temperatures, inset: digital photograph of the corresponding *N*-CQDs solution under UV-lamp (λ = 365 nm) (b) Absorption spectra of *N*-CQDs at the different reaction temperatures, (c) PL spectra of the *as*-synthesised *N*-CQDs at different citric acid: glutamine precursor molar ratio at 200 °C and (d) Absorption spectra of the *as*-synthesised *N*-CQDs at different citric acid: glutamine precursor molar ratio at 200 °C.

2.4. Fluorescent sensing and selectivity evaluation

The fluorescent sensing of metal ions using *N*-CQDs was carried out as follows. 100 μL of an aqueous *N*-CQDs solution was added to a cuvette containing 3 mL water. The fluorescent spectra of the *N*-CQDs were recorded via a spectrofluorometer at an excitation wavelength of 450 nm. For sensitivity studies, 100 μL of aqueous *N*-CQDs was added to a separate cuvette containing 3 mL ion salts of $Fe(NO_3)3$, $Co(NO_3)_2$, $Cd(NO_3)_2$, $Pb(NO_3)_2$, $Cr(NO_3)_3$, $Zn(NO_3)_2$, NaCl and KCl at 100 μM concentration. After about 5 min of incubation to ensure complete interaction between *N*-CQDs and metal ions, the fluorescent spectra of the *N*-CQDs/metal ion mixture were recorded via a spectrofluorometer. The difference in the PL intensity of the control sample (100 μL *N*-CQD in 3 mL water) with the one containing each *N*-CQDS/metal ion was recorded. To evaluate the selectivity of the *N*-CQDs towards Fe^{3+} ion, the same procedure was repeated using the mixture of an equal volume of Fe^{3+} with other interfering ions of Co^{2+}, Cd^{2+}, Pb^{2+}, Cr^{3+}, Zn^{2+}, Na^+ and K^+.

2.5. Real sample analysis

The preparation of potato (*Solanum tuberosum*) extracts was achieved via the wet digestion method. Each of the three potato tubers was grounded into a powder. Then 1.0 g of each powdered *Solanum tuberosum* was transferred to a conical flask with the addition of 1:1 HNO_3. The sample mixture was heated on an electric plate for 15 min 5 mL of concentrated HNO_3 was added with further heating for 30 min until no brown fume was given off. 2 mL of water and 30 mL of 30% H_2O_2 were added with continuous heating until the volume was reduced to less than 5 mL. Then 10 mL of HCl was added with further heating for 15 min. The sample was filtered with 0.22 μm filter paper. The solution was transferred into a 100 mL standard flask and diluted to the mark with deionized water. The calibration plot was determined using the standard addition method. The pH was adjusted to 6 using 1 M NaOH. For Fe^{3+} ions analysis, 3 mL of each of the resultant solution was added to 100 μL of the *N*-CQDs in a cuvette. The fluorescent spectra were recorded at an excitation wavelength of 450 nm.
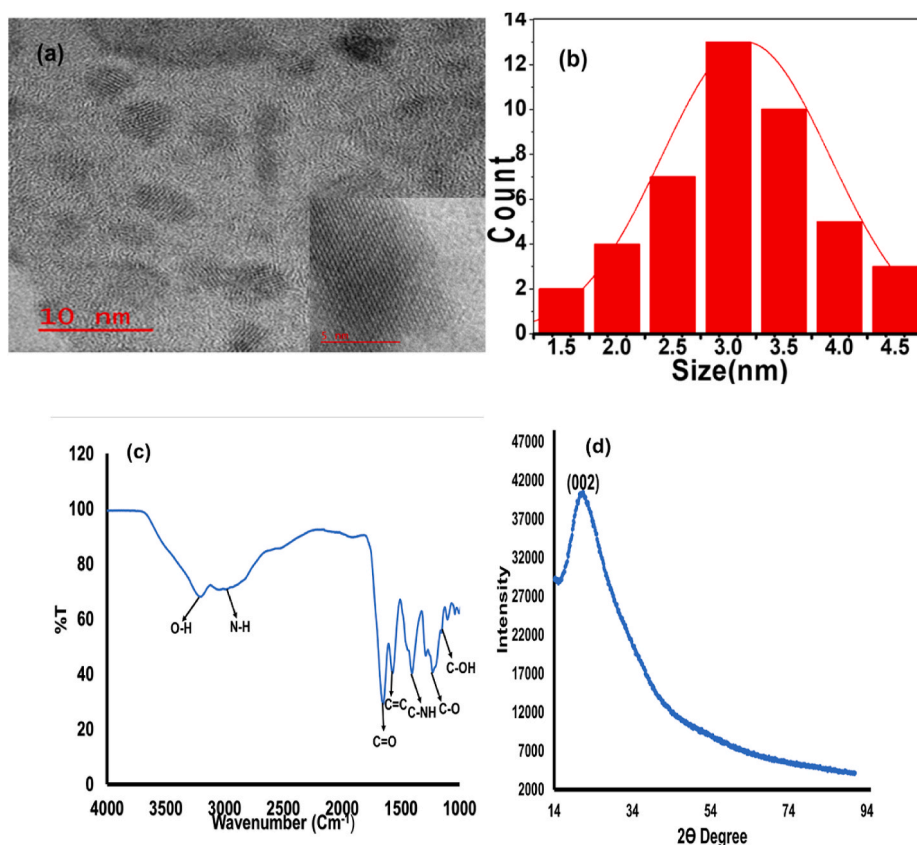
Fig. 2. (a) TEM images of as-prepared *N*-CQDs (corresponding HRTEM insets); b)Size distribution of the *N*-CQDs; c) FTIR spectra of *N*-CQDs; d) XRD pattern of the *N*-CQDs.

3. Result and discussion

3.1. Optical properties of the N-CQDs

The glutamine-based *N*-CQD was prepared using citric acid and glutamine as the carbon and nitrogen sources, respectively. The optimum synthesis temperature and the precursors molar ratio were determined using UV–Vis absorption spectroscopy and photoluminescence spectroscopy. Fig. 1a shows the photoluminescence spectra of the *N*-CQDs at different temperatures. The emission peak position becomes red-shifted from 495 to 525 nm as the temperature increases with a minimal change between 200 and 240 °C. The photographic image under the UV irradiation (Fig. 1a inset) shows that the fluorescent emission can be tuned from the blue to green region. The fluorescent intensity increased as the temperature increased with maximum intensity at 200 °C. This has been attributed to (i) an increase in the rate of the reaction of the amide linkage connecting to the carbon core [36] and (ii) carbonization [37]. The decline in the fluorescent intensity above 200 °C could be attributed to the formation of impurities caused by the carbonization of the amine into the carbon structure due to excessive heating [38,39].

The UV absorption spectra of the *N*-CQDs at varying synthesis temperature is shown in Fig. 1b. The spectra exhibited two absorption peaks across all the temperature studied. The first at 225 nm and the second at 330 nm are attributed to the π-π* transition of the aromatic C=C bond and the n- π* transition of the C=O bond, respectively [40]. The π-π* peak was similar across the temperatures, while the n- π* peak was strong at 180, 200 and 240 °C but weak at 160 and 220 °C. The peak position was the same for 180 and 200 °C, with a higher intensity observed at 200 °C. This result is in agreement with the result obtained from the photoluminescence spectroscopy. Hence, 200 °C was used as the optimal synthesis temperature.

The optimal citric acid to glutamine precursor molar ratio was investigated at 200 °C. Fig. 1c shows the photoluminescence spectra of the *N*-CQDs at a varying molar ratios of citric acid to glutamine precursors 1:1–1:4 (1:1, 1:1.5, 1:2, 1.3, and 1:4). The results showed that the fluorescent intensity of the *N*-CQDS was enhanced with an increase in the nitrogen source. However, a decline in intensity was observed above 1:3, but the emission peak position remains unaffected. The increase in the fluorescent intensity is attributed to the formation of amide groups on the surface of the *N*-CQDs, caused by the increase in the number of nitrogen atoms. The UV absorption spectra of the *N*-CQDs at a varying molar ratio of citric acid to glutamine are shown in Fig. 1d. The n- π* peak at 330 nm was weak for ratios 1:1, 1:1.5, and 1:2 but strong for ratios 1:3 and 1:4; with a more intense peak at 1:3. The results suggest that a change in the molar ratio of the precursors influences the type and numbers of functional groups present on the surface of the *N*-CQDs. The molar precursor ratio (citric acid and glutamine) of 1:3 was used for further analysis.

3.2. Morphology and structural properties of the N-CQDs

The morphological and structural properties of the *as*-synthesised *N*-CQDs were investigated using HRTEM, FTIR, and XRD. The typical HRTEM micrograph (Fig. 2a) of the *as*-synthesised *N*-CQDs at optimised synthesis conditions (200 °C and 1:3 C G) shows that they are quasi-spherical in shape and uniformly dispersed. The presence of lattice fringes (inset) confirmed the crystallinity of the as-synthesised *N*-CQDs with d-spacing (0.21 nm) aligning with (002) lattice planes of graphite. Fig. 2b shows the particle size distribution of the *N*-CQDs with an average size of 3.41 ± 0.76 nm. The FTIR spectra (Fig. 2c) show the functional groups present in the *N*-CQDs.
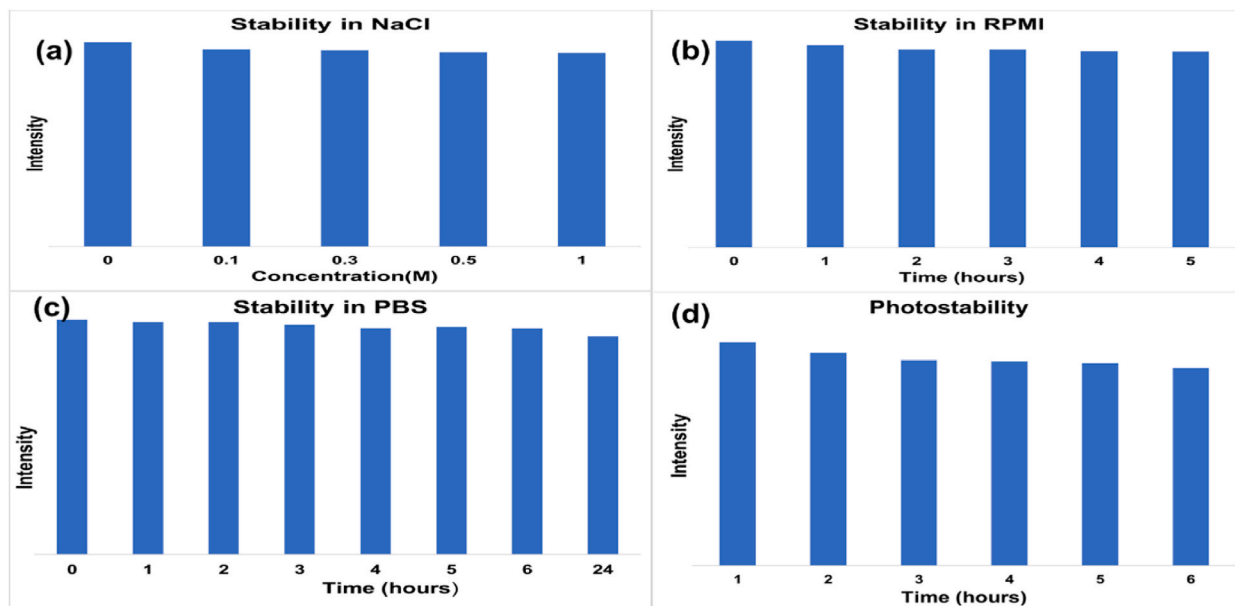

Fig. 3. Media stability in a) NaCl; b) RPMI; c) PBS and d) photostability of the developed *N*-CQDs.

The peak observed at 3184 cm^{-1} represents the presence of O–H stretching vibration bands, affirming the presence of carboxylic group in the N-CQDs. A weaker peak at 3092 cm^{-1} shows the presence of N–H stretching band from the conjugated amide group. The absorption band at 1649 and 1569 cm^{-1} represent C=O and C–NH groups on the surface of the N-CQDs. This suggests that the amino groups from the nitrogen source were incorporated into the N-CQDs structures. The peaks at 1414-1222 cm^{-1} are attributed to C–C, C–N, and C–O stretching vibration bands. This result affirms the synthesis of the N-CQDs. The XRD pattern (Fig. 2d) displayed a broad hump at $2\Theta = 23°$ (002 lattice graphite plane). This is indicative of an amorphous nature of N-CQDs with disordered carbon. It also indicates the presence low graphitic carbon structure.

3.3. Media stability

The stability of fluorescent nanomaterials in different aqueous media can be used to evaluate their practical application. The stability of the *as*-synthesised N-CQD was investigated in NaCl, RPMI, and PBS media (Fig. 3 a-c). The stability test in NaCl was carried out at different concentrations (0.1, 0.2, 0.5, and 1 M), while in RPMI and PBS, the stability was carried out between 0-5 h and 0–24 h, respectively. The result shows no noticeable change in the fluorescent intensity of the N-CQDs at different concentrations of NaCl (Fig. 3a). In addition, the fluorescence intensity remains stable in RPMI (Fig. 3b) and PBS(Fig. 3c). Furthermore, the photostability of the as-synthesised N-CQDs was investigated by irradiating the nanosensor with 365 nm UV light for an extended period (Fig. 3d). The result from the test showed little or no change in fluorescent intensity of the N-CQDs over the period. The excellent stability in these media makes the *as*-synthesised material a good candidate as nanoprobes in a similar environment. In addition, its stability in the natural saline medium is an advantage for its use in real-life applications.

3.4. pH effect

The effect of pH variation on the fluorescent intensity of the N-CQDs at an excitation wavelength of 450 nm was also investigated (Fig. 4). The fluorescent intensity was quenched at acidic pH of 2–3. The intensity increases gradually from pH 4–6 and reaches the maximum at pH 6. The fluorescence intensity was stable at pH 7–8, while the PL intensity started to decrease above pH 8, with no noticeable change observed at pH 9–12. The reduction in the fluorescence intensity in the acidic region could be attributed to the protonation of the amino and carboxylic functional groups on the surface of the N-CQDs. The protonated functional groups redistribute the surface electrons of the N-CQDs, leading to their agglomeration and eventually quenching their fluorescence. Similar observations had been reported [41,42]. At the alkaline pH, deprotonation of the carboxyl and amino groups occurs. As a result, a negative charge shell (protective layer) gradually forms on the N-CQDs surface. The fairly stable fluorescence experienced at pH 9–12 is attributed to this protective layer [43].

3.5. Selectivity and sensory evaluation of the N-CQDs nanosensor

The application of N-CQDs as fluorescent nanosensor has been widely studied. The presence of hydroxyl, carboxyl and amine groups on their surfaces enables them to form a coordinated complex with metal ions. The formation of this N-CQDs/metal ion complex resulted in quenching their fluorescent intensity. In this work, we studied the change in the fluorescent properties of the *as*-synthesised N-CQDs after the addition of various metal ion salts. The quenching of PL intensity of the N-CQDs in the presence of various metal ion salts at 450 nm is shown in Fig. 5a. A significant quenching of the fluorescent intensity of the N-CQDs was observed in the presence of Fe^{3+} at 450 nm excitation while other metal ions showed little or no influence on the PL intensity of the N-CQDs. The fluorescent quenching by Fe^{3+} may be due to the non-luminescent coordination interaction between Fe^{3+} and the hydroxyl or carboxyl group present on the N-CQDs surface. The formed hydroxy or carboxyl complex alters the electronic structure of N-CQDs. This alteration influences the movement and distribution of electrons to form a non-radioactive/hole recombination resulting in the quenching of the fluorescent intensity of the N-CQDs [44,45].

To evaluate the selectivity of the N-CQDs toward Fe^{3+}, a mixture of Fe^{3+} ions with other interfering ions was added to an aqueous
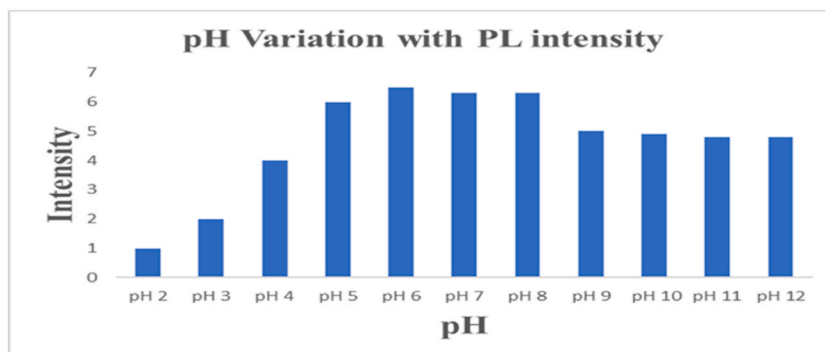

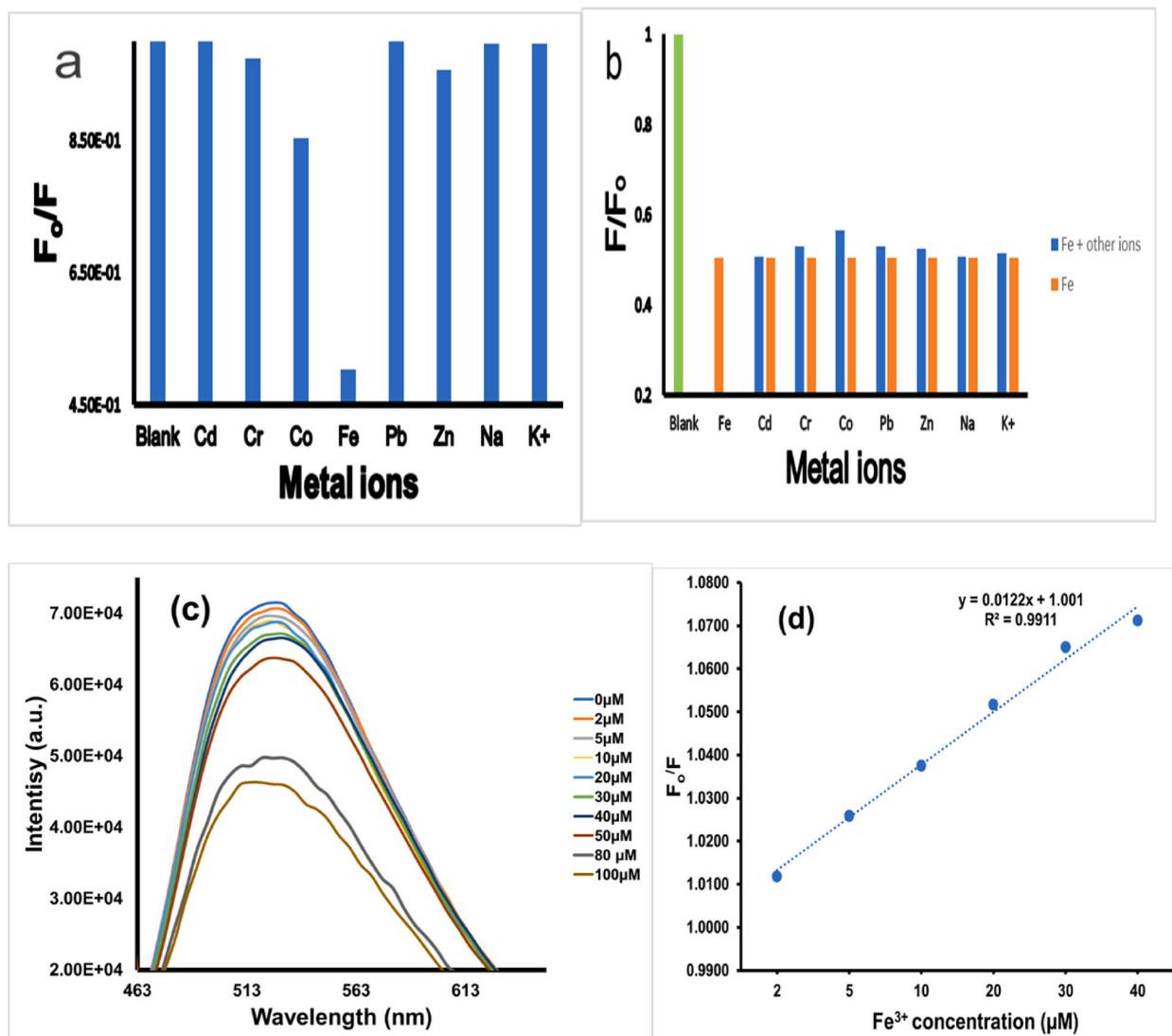**Fig. 4.** pH variation with PL intensity of the developed N-CQDs.

Fig. 5. (a) PL intensity of N-CQDs in the presence of different metal ions, (b) PL intensity of N-CQDs in the presence of Fe^{3+} and other interfering ions, (c) PL intensity of N-CQDs at different Fe^{3+} concentrations (0–100 μM), and (d) Stern-Volmer plot (linear range 2–40 μM).

solution containing N-CQDs. The result in Fig. 5b indicates that the quenching experienced was due to the effect of Fe^{3+} on the N-CQDs only. Other ions in the solution did not affect the fluorescence. This affirms the selectivity of the as-synthesised N-CQDs towards Fe^{3+} and the possible application of this fluorescent nanoprobe to determine Fe^{3+} in actual complex samples.

Table 1
Fe^{3+} determination using different nanosensors.

Probe	Precursor	Principle	Linear Range (μM)	LOD (μM)	References
N-CQDs	Malic acid/Urea	Static/IFE quenching	5–60	1.9	[47]
KBN-CQDS	*Poa Pratensis* (Kentucky bluegrass)	Formation of coordination complex	5–25	1.4	[48]
N-CQDs	Gluthamic acid and Ethylenediamine	Static quenching	8–80	3.8	[49]
N-CQDs	Lactic acid and ethylenediamine	Not stated	25–175	1.89	[50]
CQDs	Roasted chickpeas	Static quenching	11.25–37.5	2.74	[51]
Benzothiazole based sensor	Ethyl-5-benzothiazolyl-2-hydroxybenzoate	Coordination reaction	50–400	5.86	[52]
N-CQDs	Garlic skins	Dynamic quenching	0–100	4.44	[53]
N-CQDs	Citric acid and glutamine	Static quenching	2–40	1.05	This work

The sensitivity of the nanoprobe was investigated at low concentrations of Fe^{3+} in the range of 0–100 μM. The photoluminescence intensity of the *N*-CQDs decreases gradually with increasing concentration at 450 nm excitation (Fig. 5c). This suggests that the *as-synthesised N*-CQD can detect Fe^{3+} even at low concentrations. The fluorescence quenching obeys the Stern Volmer equation [46].

$$\frac{Fo}{F} = K_{sy}C + 1$$

K_{sv} -Stern -Volmer constant, *C*-concentration of quencher molecule (Fe^{3+}), F_o and F are the PL intensities of *N*-CQD at 450 nm in the absence and presence of Fe^{3+}, respectively.

The Stern-Volmer plot has good linearity with R^2 value of 0.9911 (Fig. 5d). The limit of detection was obtained using the formula $LOD = \frac{3SD}{S}$. Where SD is the standard deviation of the blank *N*-CQDs, and S is the slope of the calibration curve. The calculated limit of detection is 1.05 μM, which is low compared to those previously reported in the literature (Table 1). In addition, the synthetic procedure is simple and the developed nanosensor was used without any further functionalisation in contrast to those already reported nanosensor.

3.6. PL quenching mechanism of N-CQDs

The fluorescent quenching in carbon quantum dots by quenching molecules occurs mainly via the following mechanism; static, dynamic quenching, Förster energy resonance transfer (FRET), inner filter effect (IFE), and photo-induced electron transfer (PET) [54, 55]. A fluorescent lifetime study is a vital tool in determining if the mechanism is either static or dynamic [56,57]. If the fluorescent lifetime values of the *N*-CQDs in the presence and absence of the quencher molecule are similar, then it is static quenching; otherwise, it is dynamic quenching [58,59]. To investigate the quenching behaviour of the *N*-CQDs, the fluorescent lifetime measurement was recorded with and without the quencher molecule (Fig. 6a). The average fluorescent lifetime was 7.29 ns and 7.51 ns in the presence and absence of, Fe^{3+} respectively. These results show that the presence of Fe^{3+} has minimal influence on the excited states of the *N*-CQDs. Hence the results fulfill the condition for a static process. To further elucidate the possible quenching mechanism, the UV–Vis absorption spectra of the *N*-CQDs were obtained in the presence and absence of Fe^{3+} ions. The result (Fig. 6b) showed some variations in the spectra of the *N*-CQDs with the addition of Fe^{3+}. It was observed that the intensity of the *N*-CQDs/Fe^{3+} at absorption peaks of 230 and 328 nm was enhanced. This may be attributed to the complexation between the *N*-CQDs and the Fe^{3+} ion, which is considered to meet the criteria for static quenching [60,61]. Based on these results, we propose that the mechanism governing the fluorescent quenching of *N*-CQDs by Fe^{3+} ions was mainly via the static quenching process.

3.7. Real sample analysis

The amount of Fe^{3+} ions present in three different *Solanum tuberosum* extracts was determined using the standard addition method based on a change in the fluorescence signal of the *N*-CQDs under optimised pH conditions. The amount of Fe^{3+} in the sample solutions detected by the nanoprobe was compared with an established technique, ICP-MS. The result (Table 2) showed a satisfactory level of accuracy, 92.13–96.20%. Furthermore, the *Solanum tuberosum* extract samples were spiked with different concentrations of Fe^{3+} (5, 20, and 30 μM). As shown in Table 2, the actual spiked samples agree with the amount recovered (99.23%–103.9%) with a low relative standard deviation (1.53–2.73). These results affirm the reliability and accuracy of the *N*-CQDs-based fluorescent nanosensor for detecting Fe^{3+} ions in food samples.
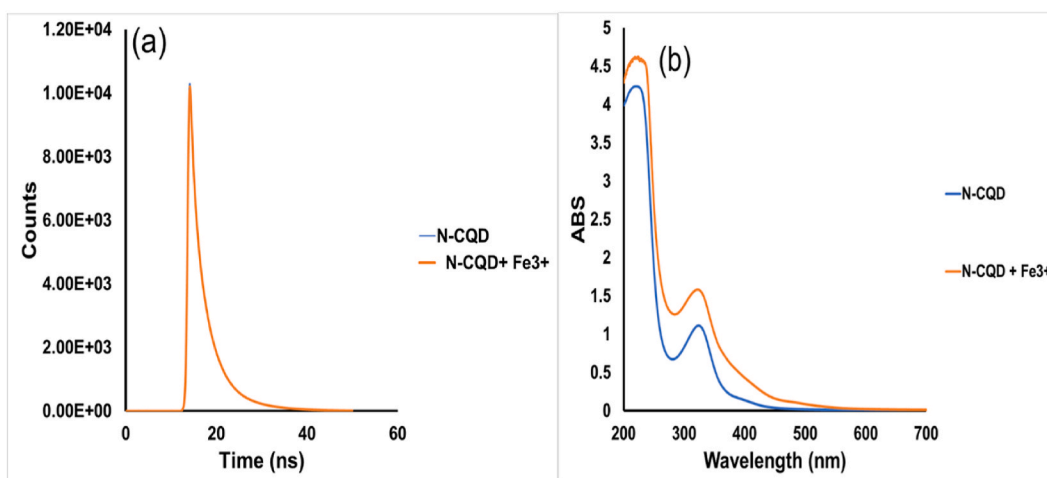

Fig. 6. (a) Fluorescence lifetime decay curve of *N*-CQDs in the absence and presence of Fe^{3+} (b) UV–Vis spectra of *N*-CQDs in the absence and presence of Fe^{3+}.

Table 2
Experimental test for Fe^{3+} determination in *Solanum tuberosum* using newly developed *N*-CQDs and ICP-MS.

Solanum tuberosum						
S/N	DetectedICP-MS (μM)	Detected *N*-CQDs (μM)	Accuracy *N*-CQDs (%)	Spiked (μM)	Found *N*-CQDs (μM)	Recovery (%)	RSD (%)
1	7.1	6.83	96.20	30	37.67	102.2	1.53
2	7.5	6.91	92.13	20	27.95	103.9	2.73
3	11.36	11.93	95.22	5	16.80	99.23	1.58

*RSD-Relative standard deviation.

4. Conclusion

In summary, a facile, fast and cost-effective method was used for the synthesis of nitrogen-doped fluorescent carbon quantum dots via a hydrothermal method using citric acid as the carbon source and glutamine as a novel nitrogen source. The temporal evolution of the optical properties of *N*-CQDs was investigated by varying the reaction temperature and citric acid: glutamine precursor ratios showed the optimal condition to be 200 °C and 1:3 precursor ratio. The as-synthesised *N*-CQDs are spherical in shape with an average particle diameter of 3.41 ± 0.76 nm and displayed green emissions. The *as*-synthesised *N*-CQDs were stable in NaCl (up to 1 M), RPMI, and PBS without any notable change in fluorescent intensity. However, the *N*-CQDs was sensitive to pH changes as the fluorescent intensity quenches in the acidic and alkaline region. The FTIR confirms the presence of carboxyl, hydroxy and amino groups on the surface of the *N*-CQDs. This was responsible for their Fe^{3+} sensing ability through the formation of Fe^{3+}/amide and Fe^{3+}/carboxyl coordination complex. Under optimised conditions, the *N*-CQDs showed selectivity towards Fe^{3+} in the presence of interfering ions with a low detection limit of 1.05 μM. The mechanism of quenching, as shown by the fluorescent decay lifetime and UV–Vis spectrum, indicates static quenching mechanism. The as-synthesised *N*-CQDs were used in practical application as a fluorescent probe to determine the amount of Fe^{3+} in *Solanum tuberosum* (Potatoes). The result closely resembled that obtained from inductively coupled mass spectroscopy (ICPMS); an established procedure with high accuracy (92.13%–96.20%). Furthermore, excellent recovery (99.23%–103.9%) was recorded when the *N*-CQDs detected samples were spiked with known concentrations of Fe^{3+} ions. This validated the reliability and accuracy of the developed fluorescent nanosensor for determining Fe^{3+} in actual food samples. This method is facile and environmentally friendly, and the as-synthesised *N*-CQDs can be employed to rapidly determine the amount of Fe^{3+} ion in actual food samples.

Author contribution statement

Olanrewaju A. Aladesuyi: Conceived and designed the experiments; Performed the experiments; Analyzed and interpreted the data; Wrote the paper.

Oluwatobi Samuel Oluwafemi: Conceived and designed the experiments; Analyzed and interpreted the data; Contributed reagents, materials, analysis tools or data; Wrote the paper.

Data availability statement

Data will be made available on request.

Declaration of competing interest

The authors declare that they have no known competing financial interests or personal relationships that could have appeared to influence the work reported in this paper.

Acknowledgement

References

[1] E. Prabhakar, Iron in cell metabolism and disease, in: M. Zakaria, T. Hassan (Eds.), Iron Metabolism - A Double-Edged Sword, IntechOpen, 2022, https://doi.org/10.5772/intechopen.101908.
[2] S.B. Kumar, S.R. Arnipalli, P. Mehta, S. Carrau, O. Ziouzenkova, Iron deficiency anemia: efficacy and limitations of nutritional and comprehensive mitigation strategies, Nutrients 14 (2022) 2976, https://doi.org/10.3390/nu14142976.
[3] K.P. Abhilash, J.J. Arul, D. Bala, Fatal overdose of iron tablets in adults, Indian J. Crit. Care Med. 17 (5) (2013) 311–313, https://doi.org/10.4103/0972-5229.120326.
[4] O. Oshin, D. Kireev, H. Hlokhova, F. Idachaba, D. Akinwande, A. Atayero, Graphene-based biosensor for early detection of iron deficiency, Sensors 20 (13) (2020) 3688, https://doi.org/10.3390/s20133688.

[5] V. Kumar, P.K. Bharti, M. Talwar, A.K. Tyagi, P. Kumar, Studies on high iron content in water resources of Moradabad district (UP), India, Water Science 31 (1) (2017) 44–51, https://doi.org/10.1016/j.wsj.2017.02.003.

[6] F.R. Adolfo, P.C. do Nascimento, G.C. Leal, D. Bohrer, C. Viana, L.M. de Carvalho, A.N. Colim, Simultaneous determination of iron and nickel as contaminants in multimineral and multivitamin supplements by solid sampling HR-CS GF AAS, Talanta 195 (2019) 745–751, https://doi.org/10.1016/j.talanta.2018.12.010.

[7] J. Kruszewska, J. Sikorski, J. Samsonowicz-Gorski, A CE-ICP-MS/MS method for the determination of superparamagnetic iron oxide nanoparticles under simulated physiological conditions, Anal. Bioanal. Chem. 412 (2020) 8145–8153, https://doi.org/10.1007/s00216-020-02948-3.

[8] S.H. Nannuri, S. Singh, S. Chidangil, S.D. George, Fluorescence-based detection of mercury ions using carbon dots: role of synthesis route, Mater. Technol. 37 (2022) 2893–2906, https://doi.org/10.1080/10667857.2022.2085441.

[9] L. Lan, Q. Niu, T. Li, A highly selective colorimetric and ratiometric fluorescent probe for instantaneous sensing of Hg^{2+} in water, soil and seafood and its application on test strips, Anal. Chim. Acta 1023 (2018) 105–114, https://doi.org/10.1016/j.aca.2018.03.023.

[10] D. Svechkarev, A.M. Mohs, Organic fluorescent dye-based nanomaterials: advances in the rational design for imaging and sensing applications, Curr. Med. Chem. 26 (21) (2019) 4042–4064, https://doi.org/10.2174/0929867325666180226111716.

[11] S. Mehta, Y. Zhang, R.H. Roth, et al., Single-fluorophore biosensors for sensitive and multiplexed detection of signalling activities, Nat. Cell Biol. 20 (2018) 1215–1225, https://doi.org/10.1038/s41556-018-0200-6.

[12] Y. Yoon, P.L. Truong, D. Lee, S.H. Ko, Metal-Oxide nanomaterials synthesis and applications in flexible and wearable sensors, ACS Nanoscience Au 2 (2) (2022) 64–92, https://doi.org/10.1021/acsnanoscienceau.1c00029.

[13] Y. Sun, W. He, X. Sun, B. Liu, MoS_2 quantum dots as a specific fluorescence sensor for selection of rutin and for temperature sensing, Luminescence 35 (8) (2020) 1416–1423, https://doi.org/10.1002/bio.3906.

[14] X. Yang, Y. Zhuo, S. Zhu, Y. Luo, Y. Feng, Y. Dou, Novel and green synthesis of high-fluorescent carbon dots originated from honey for sensing and imaging, Biosens. Bioelectron. 60 (2014) 292–298, https://doi.org/10.1016/j.bios.2014.04.046.

[15] N. Wang, Y. Wang, T. Guo, T. Yang, M. Chen, J. Wang, Green preparation of carbon dots with papaya as carbon source for effective fluorescent sensing of Iron (III) and Escherichia coli, Biosens. Bioelectron. 85 (2016) 68–75, https://doi.org/10.1016/j.bios.2016.04.089.

[16] N. Murugan, M. Prakash, M. Jayakumar, A. Sundaramurthy, A.K. Sundaramoorthy, Green synthesis of fluorescent carbon quantum dots from Eleusine coracana and their application as a fluorescence 'turn-off' sensor probe for selective detection of Cu^{2+}, Appl. Surf. Sci. 476 (2019) 468–480, https://doi.org/10.1016/j.apsusc.2019.01.090.

[17] T. Kong, L. Hao, Y. Wei, X. Cai, B. Zhu, Doxorubicin conjugated carbon dots as a drug delivery system for human breast cancer therapy, Cell Prolif. 51 (5) (2018), 12488, https://doi.org/10.1111/cpr.12488.

[18] C.G. Qian, S. Zhu, P.J. Feng, Y.L. Chen, J.C. Yu, X. Tang, Y. Liu, Q.D. Shen, Conjugated polymer for fluorescence imaging and sensing of neurotransmitter dopamine in living cells and brains of Zebrafish larvae, ACS Appl. Mater. Interfaces 7 (33) (2015) 18581–18589, https://doi.org/10.1021/acsami.5b04987.

[19] M. Bhatt, S. Bhatt, G. Vyas, I.H. Raval, S. Haldar, P. Paul, Water-dispersible fluorescent carbon dots as bioimaging agents and probes for Hg^{2+} and Cu^{2+} ions, ACS Appl. Nano Mater. 3 (7) (2020) 7096–7104, https://doi.org/10.1021/acsanm.0c01426.

[20] D. Saini, A.K. Garg, C. Dalal, S.R. Anand, S.K. Sonkar, A.K. Sonker, G. Westman, Visible-light promoted photocatalytic applications of carbon dots: a review, ACS Appl. Nano Mater. 5 (3) (2022) 3087–3109, https://doi.org/10.1021/acsanm.1c04142.

[21] Y. Yao, H. Zhang, K. Hu, G. Nie, Y. Yang, Y. Wang, X. Duan, S. Wang, Carbon dots based photocatalysis for environmental applications, J. Environ. Chem. Eng. 10 (2) (2022), 107336, https://doi.org/10.1016/j.jece.2022.107336.

[22] X. Hu, Y. Li, Y. Xu, Z. Gan, X. Zou, J. Shi, X. Huang, Z. Li, Y. Li, Green one-step synthesis of carbon quantum dots from orange peel for fluorescent detection of Escherichia coli in milk, Food Chem. 339 (2021), 127775, https://doi.org/10.1016/j.foodchem.2020.127775.

[23] R. Atchudan, T.N.J.I. Edison, K.R. Aseer, S. Perumal, N. Karthik, Y.R. Lee, Highly fluorescent nitrogen-doped carbon dots derived from Phyllanthus acidus utilized as a fluorescent probe for label-free selective detection of Fe^{3+} ions, live cell imaging and fluorescent ink, Biosens. Bioelectron. 99 (2018) 303–311.

[24] R. Atchudan, T.N.J.I. Edison, D. Chakradhar, S. Perumal, J. Shim, Y.R. Lee, Facile green synthesis of nitrogen-doped carbon dots using Chionanthus retusus fruit extract and investigation of their suitability for metal ion sensing and biological applications, Sensor. Actuator. B Chem. 246 (2017) 497–509, https://doi.org/10.1016/j.snb.2017.02.119.

[25] S. Tao, Y. Song, S. Zhu, J. Shao, B. Yang, A New Type of Polymer Carbon Dots with High Quantum Yield: from Synthesis to Investigation on Fluorescence Mechanism Polymer, vol. 116, 2017, pp. 472–478, https://doi.org/10.1016/j.polymer.2017.02.039.

[26] V. Naik, P. Zantye, D. Gunjal, A. Gore, P. Anbhule, M. Kowshik, S. V Bhosale, Govind Kolekar, Nitrogen-doped carbon dots via hydrothermal synthesis: naked eye fluorescent sensor for dopamine and used for multicolor cell imaging, ACS Appl. Bio Mater. 2 (5) (2019) 2069–2077, https://doi.org/10.1021/acsabm.9b00101.

[27] R. Atchudan, S.C. Kishore, P. Gangadaran, T.N.J.I. Edison, S. Perumal, R.L. Rajendran, M. Alagan, S. Al-Rashed, B.C. Ahn, Y.R. Lee, Tunable fluorescent carbon dots from biowaste as fluorescence ink and imaging human normal and cancer cells, Environ. Res. 204 (2022), 112365, https://doi.org/10.1016/j.envres.2021.112365.

[28] R. Atchudan, T.N.J.I. Edison, S. Perumal, N. Muthuchamy, Y. R Lee, Hydrophilic nitrogen-doped carbon dots from biowaste using dwarf banana peel for environmental and biological applications, Fuel 275 (2020), 117821, https://doi.org/10.1016/j.fuel.2020.117821.

[29] X. Deng, Y. Feng, H. Li, Z. Du, Q. Teng, H. Wang, N-doped carbon quantum dots as fluorescent probes for highly selective and sensitive detection of Fe3+ ions, Particuology 41 (2018) 94–100, https://doi.org/10.1016/j.partic.2017.12.009.

[30] L. Zhao, Y. Wang, X. Zhao, Y. Deng, Y. Xia, Facile synthesis of nitrogen-doped carbon quantum dots with chitosan for fluorescent detection of Fe^{3+}, Polymers 11 (2019) 1731, https://doi.org/10.3390/polym11111731.

[31] G. Burgos, T. Zum Felde, C. Andre andS. Kubow, The potato and its contribution to the human diet and health, in: H. Campos, O. Ortiz (Eds.), The Potato Crop, Springer, Cham, 2020, https://doi.org/10.1007/978-3-030-28683-5_2.

[32] T.R. Ziegler, A.K. May, G. Hebbar, A.K. Easley, D.P. Griffith, N. Dave, B.R. Collier, G.A. Cotsonis, L. Hao, T. Leong, A.K. Manatunga, E.S. Rosenberg, D.P. Jones, G.S. Martin, G.L. Jensen, H.C. Sax, K.A. Kudsk, J.R. Galloway, H.M. Blumberg, M.E. Evans, P.E. Wischmeyer, Efficacy and safety of glutamine-supplemented parenteral nutrition in surgical ICU patients: an American multicenter randomized controlled trial, Ann. Surg. 263 (4) (2016) 646–655, https://doi.org/10.1097/SLA.0000000000001487.

[33] H. Shabbir, T. Tokarski, D. Ungor, M. Wojnicki, Eco friendly synthesis of carbon dot by hydrothermal method for metal ions salt identification, Materials 14 (24) (2021) 7604, https://doi.org/10.3390/ma14247604.

[34] S. Smagulova, M. Egorova1, A. Tomskaya, IOP Conf. Ser.: Mater. Sci. Eng., vol. 693, 2019, 012031.

[35] P.K. Yadav, S. Chandra, V. Kumar, D. Kumar, S.H. Hasan, Carbon quantum dots: synthesis, structure, properties, and catalytic applications for organic synthesis, Catalysts 13 (2023) 422, https://doi.org/10.3390/catal13020422.

[36] Z. Yi, X. Li, H. Zhang, X. Ji, W. Sun, Y. Yu, Y. Liu, J. Huang, Z. Sarshar, M. Sain, High quantum yield photoluminescent N-doped carbon dots for switch sensing and imaging, Talanta 222 (2021), 121663, https://doi.org/10.1016/j.talanta.2020.121663.

[37] X. Zhang, L. Fu, Y. Hou, N. Long, G. Zhu, X. Liao, L. Zhou, J. Lu, W. Kong, A nitrogen-doped carbon dots based fluorescent nanosensor for sensitive assay of Fe3+ ions in Dioscorea opposita Thunb, Ind. Crop. Prod. 177 (2022), 114439, https://doi.org/10.1016/j.indcrop.2021.114439.

[38] K.Yang, C.Wang, S.Ding, F. Li, and F.Tian, The effect of reaction temperature on fluorescence properties of carbon dots. In Proceedings of the International Workshop on Materials, Chemistry and Engineering (IWMCE 2018), 229-235 ISBN: 978-989-758-346-9.

[39] Y. Zhang, Y. Wang, X. Feng, F. Zhang, Y. Yang, X. Liu, Effect of reaction temperature on structure and fluorescence properties of nitrogen-doped carbon dots, Appl. Surf. Sci. 387 (2016) 1236–1246, https://doi.org/10.1016/j.apsusc.2016.07.048.

[40] Y. Hao, R. Li, Y. Liu, X. Zhang, L. Geng, S. Chen, The on–off-on fluorescence sensor of hollow carbon dots for detecting Hg^{2+} and ascorbic acid, J. Fluoresc. 33 (2023) 459–469, https://doi.org/10.1007/s10895-022-03057-5.

[41] S.H. Jin, D.H. Kim, G.H. Jun, S.H. Hong, S. Jeon, Tuning the photoluminescence of graphene quantum dots through the charge transfer effect of functional groups, ACS Nano 7 (2) (2013) 1239–1245, https://doi.org/10.1021/nn304675g.

[42] R. Wang, X. Wang, Y. Sun, One-step synthesis of self-doped carbon dots with highly photoluminescence as multifunctional biosensors for detection of iron ions and pH, Sensor. Actuator. B Chem. 241 (2017) 73–79, https://doi.org/10.1016/j.snb.2016.10.043.

[43] G. Gao, Y. Jiang, H.R. Jia, J. Yang, F.G. Wu, On-off-on fluorescent nanosensor for Fe3+ detection and cancer/normal cell differentiation via silicon-doped carbon quantum dots, Carbon 134 (2018) 232–243, https://doi.org/10.1016/j.carbon.2018.02.063.

[44] S. Qu, H. Chen, X. Zheng, J. Cao, X. Liu, Ratiometric fluorescent nanosensor based on water soluble carbon nanodots with multiple sensing capacities, Nanoscale 5 (2013) 5514–5518, https://doi.org/10.1039/C3NR00619K.

[45] H. Wu, J. Jiang, X. Gu, C. Tong, Nitrogen and sulfur co-doped carbon quantum dots for highly selective and sensitive fluorescent detection of Fe(III) ions and L-cysteine, Microchim. Acta 184 (2017) 2291–2298, https://doi.org/10.1021/acs.jafc.8b07176.

[46] Y. Song, S. Zhu, S. Xiang, X. Zhao, J. Zhang, H. Zhang, Y. Fu, B. Yang, Investigation into the fluorescent quenching behaviours and applications of carbon dots, Nanoscale 6 (2014) 4676–4682, https://doi.org/10.1039/C4NR00029C.

[47] J. Cui, X. Zhu, Y. Liu, L. Liang, Y. Peng, S. Wu, Y. Zhao, N-doped carbon dots as fluorescent "turn-off" nanosensors for ascorbic acid and Fe3+ detection, ACS Appl. Nano Mater. 5 (5) (2022) 7268–7277, https://doi.org/10.1021/acsanm.2c01170.

[48] P. Krishnaiah, R. Atchudan, S. Perumal, E.S. Salama, Y.R. Lee, B.H. Jeon, Utilization of waste biomass of poa pratensis for green synthesis of N-doped carbon dots and its application in detection of Mn^{2+} and Fe^{3+}, Chemosphere 286 (2022) 131764–131774, https://doi.org/10.1016/j.chemosphere.2021.131764.

[49] Y. Chen, X. Sun, W. Pan, G. Yu, J. Wang, Fe^{3+}-Sensitive carbon dots for detection of Fe^{3+} in aqueous solution and intracellular imaging of Fe^{3+} inside fungal cells, Front. Chem. 7 (2020) 911, https://doi.org/10.3389/fchem.2019.00911.

[50] K. Chang, Q. Zhu, L. Qi, M. Guo, W. Gao, Q. Gao, Synthesis and properties of nitrogen-doped carbon quantum dots using lactic acid as carbon source, Materials 15 (2) (2022) 466, https://doi.org/10.3390/ma15020466.

[51] A. Basoglu, U. Ocak, A. Gumrukcuoglu, Synthesis of microwave-assisted fluorescence carbon quantum dots using roasted–chickpeas and its applications for sensitive and selective detection of Fe^{3+} ions, J. Fluoresc. 30 (2020) 515–526, https://doi.org/10.1007/s10895-019-02428-7.

[52] X. Gong, X. Ding, N. Jiang, T. Zhong, G. Wang, Benzothiazole-based fluorescence chemosensors for rapid recognition and "turn-off" fluorescence detection of Fe3+ ions in aqueous solution and in living cells, Microchem. J. 152 (2020), 104351, https://doi.org/10.1016/j.microc.2019.104351.

[53] Z. Zhai, J. Xu, T. Gong, B. Cao, K. Cui, L. Hou, C. Yuan, Sustainable fabrication of N-doped carbon quantum dots and their applications in fluorescent inks, Fe (III) detection and fluorescent films, Inorg. Chem. Commun. 140 (2022), 109387, https://doi.org/10.1016/j.inoche.2022.109387.

[54] S. Zhu, Y. Song, X. Zhao, et al., The photoluminescence mechanism in carbon dots (graphene quantum dots, carbon nanodots, and polymer dots): current state and future perspective, Nano Res. 8 (2015) 355–381, https://doi.org/10.1007/s12274-014-0644-3.

[55] F. Zu, F. Yan, Z. Bai, et al., The quenching of the fluorescence of carbon dots: a review on mechanisms and applications, Microchim. Acta 184 (2017) 1899–1914, https://doi.org/10.1007/s00604-017-2318-9.

[56] P. Venugopalan, N. Vidya, Green synthesis of mango ginger (*Curcuma amada*) derived fluorescent carbon dots—a potent label-free probe for hexavalent chromium sensing in water, Spectrosc. Lett. 55 (2022) 373–388, https://doi.org/10.1080/00387010.2022.2082483.

[57] F. Noun, E.A. Jury, R. Naccache, Elucidating the quenching mechanism in carbon dot-metal interactions–designing sensitive and selective optical probes, Sensors 21 (4) (2021) 1391, https://doi.org/10.3390/s21041391.

[58] C. Long, Z. Jiang, J. Shangguan, T. Qing, P. Zhang, B. Feng, Applications of carbon dots in environmental pollution control: a review, Chem. Eng. J. 406 (2021) 126848–126868, https://doi.org/10.1016/j.cej.2020.126848.

[59] M.J. Molaei, Carbon quantum dots and their biomedical and therapeutic applications: a review, RSC Adv. 9 (2019) 6460–6481, https://doi.org/10.1039/C8RA08088G.

[60] R. Fan, J. Xiang, P. Zhou, H. Mei, Y. Li, H. Wang, X. Liu, X. Wang, Reuse of waste Myrica rubra for green synthesis of nitrogen-doped carbon dots as an "on-off-on" fluorescent probe for Fe^{3+} and ascorbic acid detection, Ecotoxicol. Environ. Saf. 233 (2022), 113350, https://doi.org/10.1016/j.ecoenv.2022.113350.

[61] J.H. Rajendran, S. Parani, V.P.R. Remya, T.C. Lebepe, R. Maluleke, S. Thomas, O.S. Oluwafemi, Selective and sensitive detection of Cu2+ ions in the midst of other metal ions using glutathione capped CuInS2/ZnS quantum dots, Phys. E Low-dimens. Syst. Nanostruct. 136 (2022), 115026, https://doi.org/10.1016/j.physe.2021.115026.